Effect of pressure on the stability, phase behaviour and transformation kinetics between structures of lyotropic lipid mesophases and model membrane systems

1998 J. Phys.: Condens. Matter 10 11499

(http://iopscience.iop.org/0953-8984/10/49/036)

J. Phys.: Condens. Matter **10** (1998) 11499–11518. Printed in the UK PII: S0953-8984(98)96516-X

Effect of pressure on the stability, phase behaviour and transformation kinetics between structures of lyotropic lipid mesophases and model membrane systems

R Winter, J Erbes, C Czeslik and A Gabke

University of Dortmund, Department of Chemistry, Physical Chemistry I, Otto-Hahn-Straße 6, D-44227 Dortmund, Germany

Received 5 June 1998

Abstract. Lipids, which provide valuable model systems for membranes, display a variety of polymorphic phases, depending on their molecular structure and environmental conditions. By use of x-ray and neutron diffraction, infrared spectroscopy and calorimetry, the temperature and pressure dependent structure and phase behaviour of several lipid systems, differing in chain configuration and headgroup structure, have been studied. Besides lamellar phases also non-lamellar phases, such as the inverted hexagonal H_{II} phase and bicontinuous cubic phases, have been investigated. Hydrostatic pressure has been used as a physical parameter for studying the stability and energetics of lyotropic mesophases, but also because high pressure is an important feature of certain natural membrane environments (e.g., marine biotopes) and because the high-pressure phase behaviour of biomolecules is of biotechnological interest. Neutron scattering in combination with the H/D contrast variation technique has been used to the study of lateral organization of phase-separated binary lipid mixtures with distinct mixing properties. Within their two-phase coexistence regions large-scale concentration fluctuations appear, and the morphology of these fluctuations can be characterized as a complex heterogeneous system of coexisting clusters having fractal-like properties. By using the pressure-jump relaxation technique in combination with time-resolved synchrotron x-ray diffraction, the kinetics of different lipid phase transformations were also investigated. The time constants for completion of the transitions are dependent on the direction of the transition, the symmetry and topology of the structures involved, and also on the pressure-jump amplitude. In several cases also intermediate structures can be detected under non-equilibrium conditions.

Abbreviations

MA: myristic acid, PA: palmitic acid, MO: monoolein, ME: monoelaidin, DMPC: 1,2-dimyristoyl-sn-glycero-3-phosphatidylcholine (di-$C_{14:0}$), DMPS: 1,2-dimyristoyl-sn-glycero-3-phosphatidylserin (di-$C_{14:0}$), DPPC: 1,2-dipalmitoyl-sn-glycero-3-phosphatidylcholine (di-$C_{16:0}$), DSPC: 1,2-distearoyl-sn-glycero-3-phosphatidylcholine (di-$C_{18:0}$), DOPC: 1,2-dioleoyl-sn-glycero-3-phosphatidylcholine (di-$C_{18:1,cis}$), DOPE: 1,2-dioleoyl-sn-glycero-3-phosphatidylethanolamine (di-$C_{18:1,cis}$), POPC: 1-palmitoyl-2-oleoyl-sn-glycero-3-phosphatidylcholine ($C_{16:0}$, $C_{18:1,cis}$), DEPC: 1,2-dielaidoyl-sn-glycero-3-phosphatidylcholine (di-$C_{18:1,trans}$); egg-PE: egg-yolk phosphatidylethanolamine, FA: fatty acid, PC: phosphatidylcholine.

1. Introduction

A rich polymorphism is one of the fascinating properties of lipid systems [1–5]. Over the years many lipid/water systems have been investigated, many mesophases have been

0953-8984/98/4911499+20$19.50

identified and their structures have largely been determined. Lipids are also the basic structural element of biological membranes which consist of a lamellar phospholipid matrix. Also these lipid bilayers exhibit a rich lyotropic and thermotropic phase behaviour. Due to the large hydrophobic effect, most phospholipid bilayers associate in water even at extremely low concentrations ($<10^{-12}$ mol l^{-1}). Saturated phospholipids often exhibit two thermotropic lamellar phase transitions, a gel to gel ($L_{\beta'}/P_{\beta'}$) pretransition and a gel to liquid-crystalline ($P_{\beta'}/L_{\alpha}$) main transition at a higher temperature T_m (see figure 1). In the fluid-like L_{α} phase, the hydrocarbon chains of the lipid bilayers are conformationally disordered, whereas in the gel phases, the chains are more extended and ordered. In addition to these thermotropic phase transitions, also pressure-induced phase transformations have been observed (see, e.g., [6–20]).

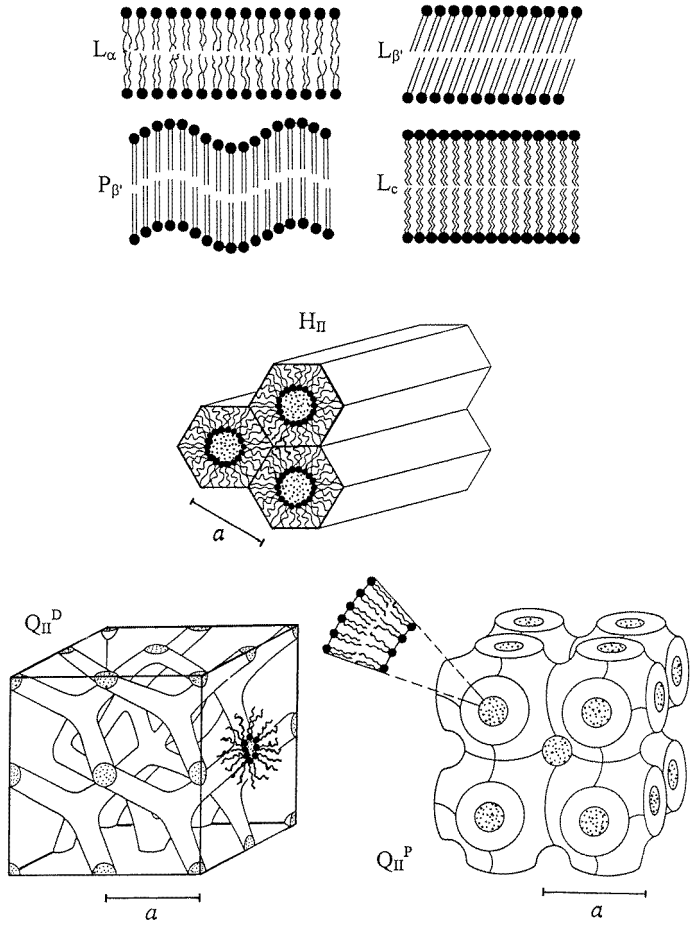

Figure 1. Schematic drawing of lamellar gel (L_c, $L_{\beta'}$ and $P_{\beta'}$) and liquid-crystalline L_{α}, inverted hexagonal (H_{II}) and two bicontinuous cubic (Q_{II}) lipid phases.

It is now well known that many biological lipid molecules also form non-lamellar liquid-crystalline phases (see figure 1) [1–5, 21–23]. For example, some lipid extracts such as those from archaebacteria (*S. solfataricus*) exhibit a cubic phase instead of a lamellar phase usually observed with lipid preparations [24, 25]. For the double-chain lipids found in membranes,

the polar/apolar interface curves toward the water (such phases are called inverse or type II). It is assumed that the non-lamellar lipid structures, such as the inverse hexagonal (H_{II}) and bicontinuous cubic lipid phases, are also of biological relevance. They probably play an important functional role in some cell processes [25–30]. Fundamental cell processes such as constitutive secretion, endo- and exocytosis, membrane recycling, protein trafficking, fat digestion and enveloped virus infection involve a rearrangement of biological membranes where non-lamellar lipid phases are probably involved, and there might be some stage of membrane fusion that depends on the distinct properties of membrane lipid bilayers. A recent reanalysis of a large number of published electron micrographs of cell membranes has shown that static cubic structures (cubic membranes) might also occur in biological cells [25, 31].

To date, seven cubic phases are known. At a macroscopic level, they are very viscous and optically isotropic. The lipid cubic phases can be sorted in two main classes: bicontinuous and micellar [1, 2, 21, 22, 32, 33]. The bicontinuous cubic phases of type II (Q_{II}) can be visualized in terms of a highly convoluted lipid bilayer, which subdivides three-dimensional space into two disjointed polar labyrinths separated by an apolar septum. The structures of three of these phases, Q^{230}, Q^{224} and Q^{229}, are closely related to the Schoen gyroid (G), the Schwarz D and the Schwarz P infinite periodic miminal surfaces (IPMSs). An IPMS is an intersection-free surface periodic in three dimensions with a mean curvature that is everywhere zero. The surface, that sits at the lipid bilayer midplane, separates two interpenetrating but not connected water networks. A prerequisite for the formation of the H_{II} or inverse cubic phases is that the opposing monolayers wish to bend towards the water region. This desire arises because of differential lateral pressures which are present through the monolayer films. It increases, for instance, if the lateral chain pressure increases due to increase of *trans/gauche*-isomerizations of the acyl chains at high temperatures or if the level of headgroup hydration decreases (e.g., due to Ca^{2+} adsorption at the polar/apolar interface). So far, no full theoretical description of lyotropic lipid phase behaviour exists, though some progress has been made in recent years [34–40]. Often a concept is used that can be explained in terms of a small set of parameters, irrespective of the precise chemical nature of the lipid molecules. Helfrich described the surface curvature energy contribution associated with amphiphile films, in terms of three curvature elastic parameters: the spontaneous mean curvature H_s, the mean curvature modulus κ_m and κ_G, the Gaussian curvature modulus [41]. For small curvatures, the surface energy per unit area is given by

$$G_{bend}/S = g_{bend} = 2\kappa_m\langle(H - H_s)^2\rangle + \kappa_G\langle K\rangle. \tag{1}$$

H is the mean interfacial curvature, which is equal to half the sum of the principal curvatures $C_1 = 1/R_1$ and $C_2 = 1/R_2$ at the interface, and K is the Gaussian curvature at the interface, given by the product of the principal curvatures C_1 and C_2. The spontaneous mean curvature H_s is that mean curvature the lipid aggregate would wish to adopt in the absence of external constraints, and κ_m tells us what energetic cost there would be for deviations away from this. Besides the curvature energetic contribution, there will be other energetic contributions. Due to the desire to fill all the hydrophobic volume by the amphiphile chains (hydrophobic effect), there will be also a contribution quantifying an eventual packing frustration. A further contribution might be due to interlamellar interactions (e.g., van der Waals interaction, hydration repulsion). The curvature elastic energy is believed to be the crucial term governing the stability of non-lamellar phases and the ability of lipid membranes to bend, in particular at high levels of hydration. To probe the concept of any energetic description and the resultant set of parameters necessary to provide a general explanation

of universal lyotropic phase behaviour, one needs to scan the appropriate parameter space experimentally.

Most of the experimental work so far has relied on temperature and sample composition as the tools to attack this problem. A further important thermodynamic variable is pressure. Besides the general physico-chemical interest in using high pressure as a tool for understanding phase behaviour, structure and energetics of amphiphilic molecules, high pressure is also of considerable physiological and biotechnological (e.g., high pressure food processing) interest [42–47]. Hydrostatic pressure significantly influences the structural properties and thus functional characteristics of cell membranes, yet this has not prevented the invasion of high-pressure, cold habitats by deep-sea organisms (up to ∼10 000 m depth, corresponding to 1 kbar of pressure at 2–3 °C). Without any compensatory adjustments the membranes of deep-sea organisms should be highly ordered. It is now well established that deep-sea organisms display a variety of adaptations to high hydrostatic pressure at the molecular level of organization to keep their membranes in a fluid-like state which is a prerequisite for optimal physiological function [47].

In this review, we present data on the temperature and pressure dependent phase behaviour, energetics and stability of single- and two-component phospholipid bilayers. Then, we discuss the pressure-jump relaxation technique for studying the kinetics of phase transformations between lyotropic mesophases. We will mainly focus on the discussion of experimental results. For the investigation of the high-pressure phase behaviour and structure of lipid systems, as well as the kinetics of lipid phase transitions using the pressure-jump technique, we built high-pressure x-ray cells using Be or diamond windows. Details of the experimental techniques are discussed elsewhere [48, 49]. The small- and wide-angle part of the diffraction pattern has been measured simultaneously. In the small-angle x-ray scattering (SAXS) region of model membranes, Bragg reflections of first order occur ($s_{001} = 1/d_{001} = 1/a$) indicating a lamellar packing of the lipid bilayers in the form of multilamellar vesicles ($s = (2/\lambda)\sin\theta$, λ wavelength of radiation, 2θ scattering angle). The repeat distance of the lamellar lattice constant a is the sum of the lipid bilayer thickness and the thickness of one adjacent interlamellar water layer. In the wide-angle x-ray scattering (WAXS) region the packing of the lipid acyl chains is detected. In the gel phase, the chain lattice is normally either of an undistorted or a distorted hexagonal type. Assuming a hexagonal packing of the lipid acyl chains, reflections occur at $s_{11} = s_{20} = 1/d_{hex} = 2/(\sqrt{3}\,a_{hex})$ where a_{hex} is the distance between two acyl chains. A distorted hexagonal or orthorhombic lattice of the lipid acyl chains has two reflections in the wide-angle region: a sharp reflection at $(1/d_{20})$ and an usually broad one at $(1/d_{11})$. The orthorhombic lattice parameters a_{orth} and b_{orth} of the chain packing can be calculated using $a_{orth} = 2d_{20}$ and $b_{orth} = d_{11}/[1 - (d_{11}/2d_{20})^2]^{1/2}$. The area per chain perpendicular to the chain axis is given by $A = a_{orth}b_{orth}/2$. In the fluid, liquid-crystalline phase, only a diffuse broad high-angle reflection is observed centred around 1/(4.5 Å), which is indicative of disordered chains.

To decipher the conformational differences of the various mesophases, we have applied Fourier-transform infrared (FTIR) spectroscopy. Vibrational spectra of lipid systems consist of bands arising from the transitions between vibrational energy levels of various types of intramolecular and intermolecular vibrations in the ground electronic state. Many infrared spectral parameters, particularly the frequencies, widths, intensities, shapes and splittings of the IR bands, are very sensitive to the structural and dynamical properties of membrane lipid molecules [11, 50]. In particular cases, such as by analysing the CH_2 wagging vibrations, even quantitative conformational information on conformer population can be obtained.

2. Results and discussion

2.1. Phase transitions of single-component phospholipid bilayer dispersions

2.1.1. Lamellar phase transitions. The increase in entropy with chain rotational disorder, together with the increase in intermolecular entropy and the increased headgroup hydration, are the driving forces for the $L_{\beta'}(P_{\beta'})/L_\alpha$ chain melting transition. Opposing the chain melting is the increase in internal energy due to increased rotational isomerism, the decreased van der Waals attraction between chains, and the increased hydrophobic exposure at the polar/apolar interface that results from the lateral expansion of the bilayer accompanying the increase of chain isomerism. The balance of these opposing contributions to the bilayer free energy, which depends on the geometry of the lipid molecule, determines the chain melting transition temperature T_m. Generally, the lamellar gel phases prevail at high pressure and low temperature. They give way to the lamellar liquid-crystalline L_α phase as pressure is lowered and temperature is raised. A common value for the L_α/gel transition slope of about 22 °C kbar^{-1} has been observed for the saturated phosphatidylcholines DMPC, DPPC and DSPC [6-13] (see figure 2; for abbreviations see above). The positive slope can be explained by the endothermic enthalpy change ΔH_m and the volume increase ΔV_m at the gel to L_α transition through the Clapeyron relation $\mathrm{d}T_m/\mathrm{d}p = T_m\Delta V_m/\Delta H_m$. Similar transition slopes have been found for the mono-*cis*-unsaturated POPC, the phosphatidylserine DMPS, and for the phosphatidylethanolamine DPPE. Only those of *cis*-unsaturated DOPC and DOPE have been found to be markedly smaller [6, 11]. The transition slope does not significantly depend on the hydrocarbon chain length or the type of headgroup; they affect the transition temperature, mainly. The existence of *cis* double bonds in the chain region drastically affects the transition slope, however. The introduction of *cis* double bonds leads to the lowest transition temperatures and smallest transition slopes, presumably as they impose a kink in the linearity of the acyl chains, thus creating significant free volume in the bilayer, which reduces the ordering effect of high pressure. Also further pressure-induced

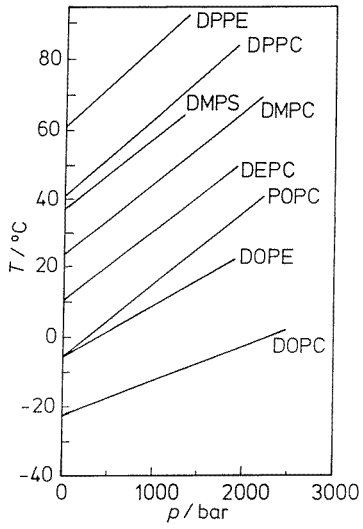

Figure 2. T, p phase diagram for the main (chain-melting) transition of different phospholipid bilayer systems. The L_α phase is observed at the low-pressure high-temperature corner of the phase diagram.

gel phases have been observed in single-component phospholipid dispersions, such as an interdigitated high-pressure gel phase in DPPC and DSPC [7, 8]. These studies clearly demonstrate that, by regulating the lipid composition of the cell membrane through changes in lipid chain length, degree of unsaturation and headgroup structure, biological organisms are already provided with a mechanism for efficiently modulating the physical state of their membranes in response to changes in the external environment ('homeoviscous adaptation'), such as high hydrostatic pressure in the deep sea [6, 47]. However, nature has also further means to regulate membrane fluidity, such by changes in concentration of cholesterol and protein in the lipid bilayer [6, 15, 51].

2.1.2. Non-lamellar phase transitions. For a series of lipid molecules, also non-lamellar phases occur as thermodynamically stable phases or they can often be induced as long-lived metastable states. Here we discuss three examples, taken from different groups of amphiphilic molecules. In contrast to DOPC, the corresponding *cis*-unsaturated phospholipid with ethanolamine as headgroup, DOPE, in addition to the lamellar L_β/L_α transition exhibits a lamellar L_α to inverted hexagonal (H_{II}) transition. As pressure forces a closer packing of the chains, which results in a reduction of the number of gauche bonds within the chains, both transition temperatures increase with increasing pressure. As an example of x-ray experimental data in the diamond pressure cell, figure 3 shows diffraction patterns of a DOPE dispersion (70 wt% H_2O) at 15 °C and several pressures. As a function of pressure, the diffraction patterns of the H_{II} phase, the L_α phase and of two lamellar gel structures L_β^h, L_β^o with different packing properties of the acyl chains are seen [52]. The single wide-angle reflection of the L_β^h structure points to a hexagonal packing of the lipid chains. Increase of pressure leads to the appearance of two wide-angle peaks. They might be ascribed to the Miller indices (20) and (11) of a two-dimensional orthorhombic lattice where the chains are tilted. The drastic decrease of the (001) lamellar spacing by 6.5 Å also indicates the formation of a tilted gel structure. At pressures above about 10 000 bar the lamellar lattice constant further decreases as the interlamellar bulk water freezes (the freezing point of bulk water at 15 °C is at about 8000 bar). The chain cross sectional area as determined from the wide-angle reflections is ∼24 $Å^2$ in the L_α phase, 20.9 $Å^2$ in the pressure-induced L_β^h phase

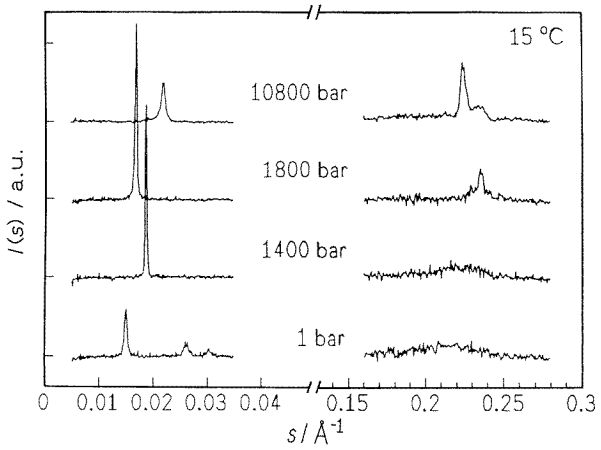

Figure 3. SAXS and WAXS patterns of DOPE in excess water for selected pressures at $T = 15$ °C.

at 1600 bar and it increases again in the L_β^o tilted ($\sim 30^\circ$) gel phase (22.7 Å^2 at 2500 bar, 21.2 Å^2 at 20 400 bar). Figure 4 displays the corresponding T,p phase diagram obtained. The transition slope of the H_{II}/L_α transition ($dT_h/dp \approx 40\,^\circ$C kbar^{-1}) is almost three times as steep as the slope of the lamellar chain-melting transition ($dT_m/dp \approx 14\,^\circ$C kbar^{-1}). A similar steep slope for the H_{II}/L_α transition has also been observed for egg-PE [6, 53]. The H_{II}/L_α transition is the most pressure-sensitive lipid phase transition found to date.

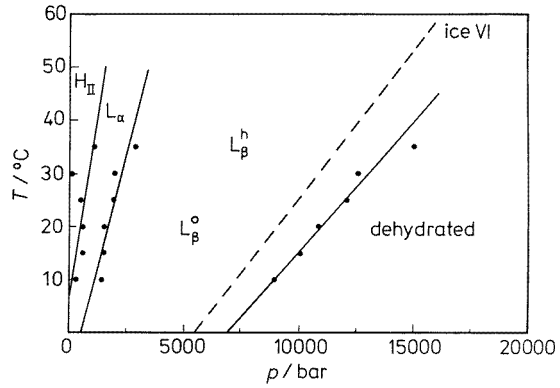

Figure 4. T,p phase diagram of DOPE in excess water.

In DOPE also two cubic phases Q_{II}^D, Q_{II}^P of space group $Pn3m$ and $Im3m$, respectively, can be induced by subjecting the sample to an extensive temperature or pressure cycling process at conditions close to the transition region of the L_α and H_{II} phase [6, 23, 54]. Figure 5(a) displays diffraction patterns of a pressure-cycled DOPE dispersion. The Bragg reflections (10), (11) and (20) of the H_{II} phase, the (001) and (002) reflections of the L_α phase and the Bragg peaks of the cubic structures of space group $Im3m$ and $Pn3m$ are seen. Figure 5(b) shows the diffraction pattern of a DOPE dispersion after 1400 temperature cycles between $-5\,^\circ$C and $15\,^\circ$C. It is also possible to induce metastable cubic structures in naturally derived lipid systems. Dispersions of egg-PE in excess water spontaneously form a lamellar L_β, L_α and a H_{II} structure with increasing temperature, and no equilibrium cubic phase is found (figure 6). However, after a series of pressure-jumps passing the H_{II}/L_α transition we observe the formation of additional metastable cubic phases of space groups $Im3m$ (Q_{II}^P), $Pn3m$ (Q_{II}^D) and $Ia3d$ (Q_{II}^G) (figure 7). Indeed, application of high pressure seems to be an effective way of inducing cubic structures. It has been shown that, in certain situations, the topology of bicontinuous cubic phases can result in a similar or even lower free energy than either the lamellar L_α or H_{II} phase, as the cubic phases have low curvature energies and do not suffer the extreme chain packing stress of the H_{II} phase. The metastable cubic structures might be formed via defect structures which occur when passing the L_α/H_{II} transition, such as interlamellar micellar intermediates and stalks [27, 55]. A stalk is a neck-like structure connecting only the contacting monolayers of the membranes. Also membrane fusion in diverse biological fusion reactions probably involves formation of some specific intermediates, such as stalks and pores, and the energy of these intermediates, and, consequently, the rate and extent of fusion depend on the propensity of the corresponding monolayers of membranes to bend. Lipid composition may be altered by enzymatic (fusion proteins) attack. From a membrane point of view, to be best suited for fusion, membranes should be asymmetrical, with the contracting monolayers containing H_{II} phase-promoting lipids (e.g., cholesterol, PEs with negative H_s), and with the inner

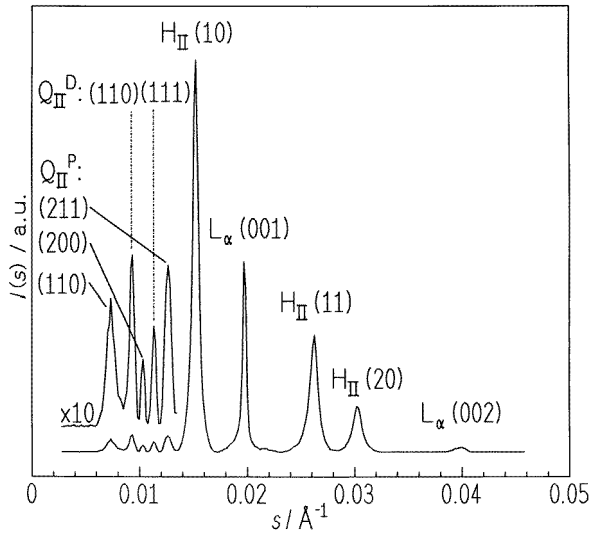

(a)

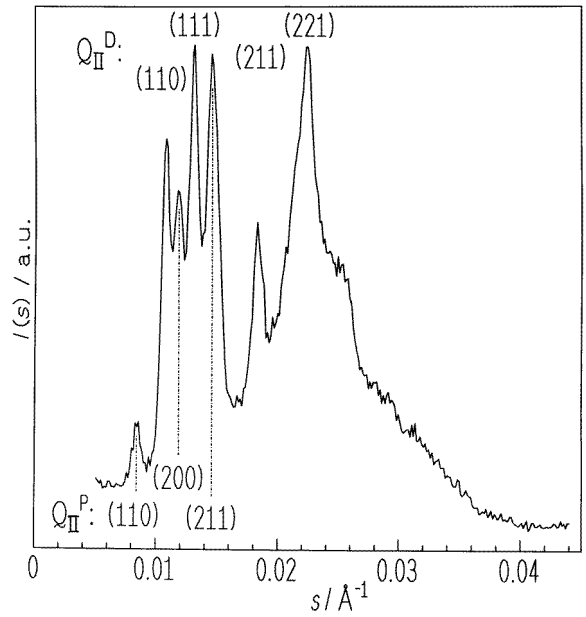

(b)

Figure 5. SAXS patterns of DOPE/excess water, which has been (a) pressure cycled between the L_α and H_{II} phase, and (b) temperature cycled 1400 times (using a roboter-type apparatus) across the L_α to H_{II} phase transition.

(distal) monolayers containing micelle-forming lipids (e.g., lysolipids).

Fourier-transform infrared spectroscopy has been used to characterize differences in conformation and hydration between different lamellar and non-lamellar phases of the single-chain lipid monoelaidin (ME) in excess water [50] and, in combination with synchrotron

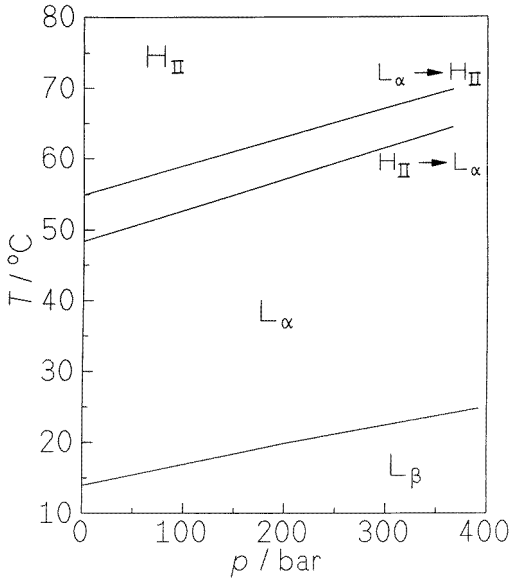

Figure 6. T,p phase diagram of egg-PE in excess water.

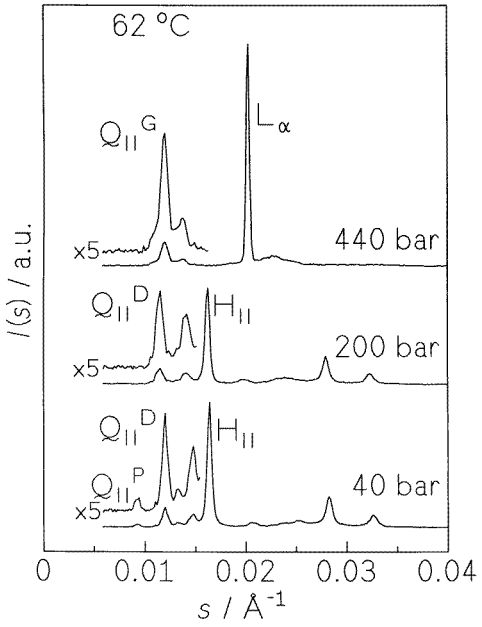

Figure 7. SAXS patterns of egg-PE/excess water which has been pressure cycled between 30 and 450 bar at 62 °C.

x-ray diffraction results [16], to establish the T,p phase diagram of the system over an extended temperature and pressure range (figure 8). Increasing the temperature will introduce greater disorder in the hydrocarbon chain, thus leading to a larger chain splay and greater desire for the lipid interface to curve toward the aqueous region. As a

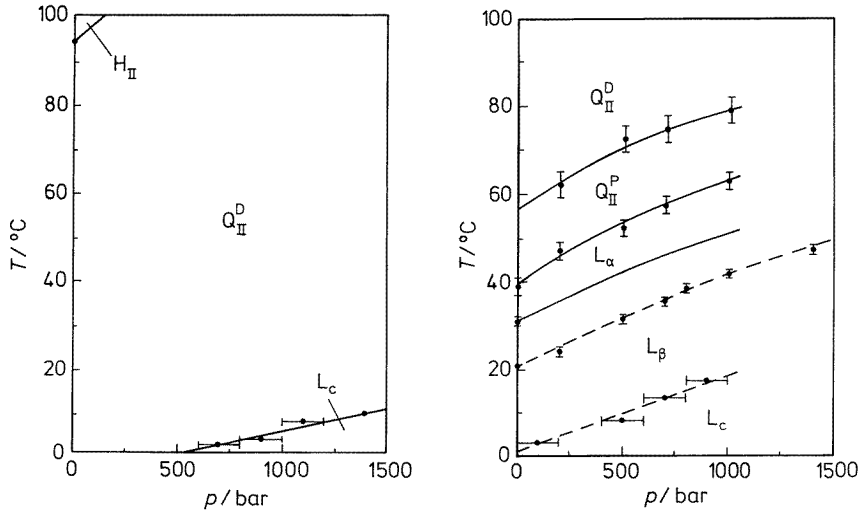

Figure 8. T, p phase diagram of (a) monoolein (MO) and (b) monoelaidin (ME) in excess water. The lamellar L_β phase of ME is probably metastable (dashed phase lines).

consequence, bicontinuous cubic phases are formed. The dominant effect of pressure will then be a straightening of the chains as the molecular volume of the system is reduced by pressurization. The L_β phase might be a metastable phase. Above 10 °C, the L_β phase is stable for days, however. At 9 °C, it exists at least 30 min, and at 4 °C, it converts to the L_c phase within 10 min. At low temperatures, the lamellar crystalline L_c phase of ME is probably the thermodynamically stable phase. In the L_c phase most molecular motions are frozen out. When heated, the L_c phase transforms to the lamellar liquid-crystalline L_α phase at about 32 °C. With continued heating, the L_α phase converts to the bicontinuous cubic phase Q^P_{II} (space group $Im3m$) at about 39 °C. At ∼55 °C, a second bicontinuous cubic phase, the Q^D_{II} (space group $Pn3m$) phase, is formed. Metastable phases can easily be induced in ME when cooling the system down from temperatures above 60 °C. The Q^D_{II} phase can be undercooled to 27 °C, and the Q^P_{II} phase appears between 29 °C and 21 °C. Further decrease of temperature leads to the formation of the L_β phase and no L_α phase is observed [52]. For comparison, figure 8 also shows the p,T phase diagram of MO in excess water. As can be clearly seen, a small change in the acyl chain configuration (a *trans* (in ME) versus *cis* (in MO) double bond at position C_9, C_{10}) leads to a significant change in acyl chain repulsive pressure and thus to drastic changes in phase behaviour.

Changes of ionic strength often has a significant effect on the structure and phase behaviour of lyotropic mesophases. For example, with increasing Ca^{2+} concentration, the lattice constant a of the Q^P_{II} phase of MO decreases whereas increase of pressure has an opposite effect, e.g. for 50 °C, 1 bar from 83.7 Å at 0.1 M $CaCl_2$ to 81 Å at 1 M $CaCl_2$, and for 50 °C and 1500 bar from 95.5 Å at 0.1 M $CaCl_2$ to 92.6 Å at 1 M $CaCl_2$ solution, respectively. Adsorption of Ca^{2+} at the polar/apolar interface probably leads to a partial dehydration of the lipid headgroup so that the lipid monolayer curvature increases and a decreases.

It is clear that an understanding of the form of the p,T phase diagram of lipid systems such as ME/water would require a detailed consideration of all the complex interactions

involved, such as interfacial, hydration and van der Waals forces, steric repulsion, hydrogen bonding, as well as the geometry of the lipid molecule as a function of the thermodynamic parameters temperature and pressure. At present, modelling of these contributions is still in its infancy, and one is not yet able to predict lyotropic phase stability and phase sequence as a function of temperature and pressure. Only selected contributions can be modelled so far. We used x-ray diffraction measurements of the variation of lattice parameters a with hydration and pressure at 50 °C of hydrated monoelaidin to calculate the curvature elastic energy contribution for the lipid Q_{II}^{G} ($Ia3d$) cubic mesophase, which is observed under limited hydration conditions. To calculate the curvature energy, the monolayer radius of curvature has been defined at the so-called neutral interface, which represents a surface which does not register a molecular cross-sectional area change upon bending by hydration. The neutral area surface is displaced from the minimal surface by a distance ξ. The cross-sectional area of a lipid molecule at a distance x from the minimal surface is given by [34, 56]

$$s(x) = \frac{2S(x)v_L}{\phi_L a^3} \tag{2}$$

with $S(x) = \sigma a^2 + 2\pi\chi x^2$ the total surface area of the monolayer, χ the Euler characteristic of the surface (-8 for the G surface), σ = area of minimal surface/(unit cell volume)$^{2/3}$ ($\sigma = 3.091$ for the G surface), v_L and ϕ_L are the molecular volume and volume fraction of the lipid, respectively. v_L can be determined by $v_L = Mv_{sp,L}/N_A$ with $v_{sp,L}$ the lipid specific volume, and M the molar mass of the lipid. Knowing ϕ_L and a from measurement we can calculate the lipid length l for a given phase [56, 57]:

$$\phi_L = (1 - \phi_w) = 2\sigma\left(\frac{l}{a}\right) + \frac{4\pi\chi}{3}\left(\frac{l}{a}\right)^3. \tag{3}$$

The volume fractions of lipid (ϕ_L) and water (ϕ_w) have been determined from the mass fraction and densities of water and ME, respectively, and the lattice constant a has been obtained from x-ray diffraction measurements [52]. Using equation (3), a value of $l = 15.1$ Å is found for ϕ_L values between 0.4 and 0.5. In measurements on MO/water, a value of $l = 17.3$ Å has been found for $T = 25$ °C [36, 38].

An appropriate neutral surface analysis involves calculating $s(x)$ at different positions along the length of the lipid molecule as a function of hydration. With increasing level of hydration, the cross-sectional area of the lipid molecule increases at the headgroup and decreases at the chain ends. The required neutral surface is located at that value of x in the cross-sectional area profile where $s(x)$ remains constant, i.e., where the profiles cross in the hydration series. At $\xi = 9.3$ Å for 50 °C and 1 bar, no change of $s(x)$ is observed. Here the neutral surface area is situated with a cross-sectional area per lipid molecule of 41.5 Å^2. Using the analysis of Templer [35, 36], ξ can be obtained in a more rigorous way. Referring to the free bending energy per surface area for the two monolayers, which can be characterized by two neutral surfaces, a distance $\pm\xi$ apart from the IMPS, one obtains

$$G_{bend}/S_0 = g_{bend} = \kappa_{G,b}\langle K_0\rangle + \kappa'_{G,b}\langle K_0^2\rangle \tag{4}$$

where $\kappa_{G,b}$ and $\kappa'_{G,b}$ are the first- and second-order Gaussian curvature moduli for the bilayer (index b), respectively, with $\kappa_{G,b} = 2\kappa_G - 8\kappa_m H_s\xi$ and $\kappa'_{G,b} = 4\kappa_m\xi^2 - (2\kappa_G - 8\kappa_m H_s\xi)\xi^2/f$ and $f = 1.2187$. From the experimental determination of a and l as a function of hydration, ξ and the ratio of the bending constants (κ_G/κ_m)

$$\frac{\kappa_G}{\kappa_m} = -\frac{8\pi\chi f\xi^2}{\sigma a^2 - 4\pi\chi\xi^2} + 4H_s\xi \tag{5}$$

can be calculated [34–36]. Here it should be pointed out again that the neutral surface is assumed to be parallel to the minimal surface, which is likely to be the case at high levels of hydration. A similar value of ξ of 9.6 to 9.7 Å can be determined using this method which is only slightly hydration dependent. This places the neutral surface at the upper part of the lipid chain which is generally believed to be the most incompressible region. Assuming that the spontaneous curvature H_s of the ME monolayers at 50 °C is similar to the mean curvature of the neutral surface, $\langle H_\xi \rangle = -5.32 \times 10^{-3}$ Å^{-1}, a value of $(\kappa_G/\kappa_m) = 0.012$ is obtained for $\phi_w = 0.49$, $\xi = 9.5$ Å and $a = 174.6$ Å. Alternatively, the bending constants can be measured using osmotic pressure [39]. A similar value of $(\kappa_G/\kappa_m) = 0.05$ has been obtained for MO/water at 25 °C using $\xi = 12.6$ Å [36]. As $\langle K_\xi \rangle < 0$, a positive value of (κ_G/κ_m) means that the free energy of the lipid system is indeed lowered upon formation of the bicontinuous cubic phase. Modifications of the free energy expression to include additional terms are being tested currently (see, e.g., [37]).

Energetic models based on first-order bending energy arguments predict that the different inverse bicontinuous cubic phases Q^G_{II}, Q^D_{II} and Q^P_{II} are energetically degenerate. In fact, this energetic degeneracy is not observed in the experimental results for establishing the p,T phase diagram of this and other lipid systems. Recently, it has been shown by Templer *et al* [37] that the energetic degeneracy of the bicontinuous cubic phases can indeed be broken by changes in the geometry of the interface. Analysis of 2:1 fatty acid/phospholipid mixtures suggests that the destabilization of Q^P_{II} with respect to Q^D_{II} as one increases the temperature may be understood in terms of the requirements for the interface to alter geometry as it goes from one of almost constant mean curvature to one which approaches a constant thickness monolayer.

2.2. Phase transitions of binary lipid mixtures

The addition of fatty acids drastically changes the phase behaviour of aqueous lecithin dispersions. Dispersions of DMPC and DPPC merely exhibit lamellar phases [3]. Non-lamellar inverted hexagonal (H_{II}) and/or inverted bicontinuous cubic phases can be induced by adding myristic acid (MA) or palmitic acid (PA), respectively [49, 58–60]. Fatty acids probably influence the fusogenicity of biological membranes because they relieve the formation of non-lamellar intermediate structures which have to occur in the process of membrane fusion. In liquid-crystalline phases of DMPC/MA and DPPC/PA 1:2 mixtures, the incorporated fatty acid molecules increase the spontaneous curvature of the lipid monolayers, so that one does not observe the lamellar liquid-crystalline phase (L_α) in equilibrium measurements: the systems show a direct transition from the lamellar L_β to non-lamellar phases. Figure 9 shows the p,T phase diagrams for the 1:2 mixtures of DMPC/MA and DPPC/PA containing 75 wt% water [49]. Both systems exhibit a phase separation into two crystalline phases at low temperatures, one of these crystalline phases consisting of the pure crystalline fatty acid (L_c) and the other of a mixture of the lecithin and the fatty acid (L_c^{com}). At ambient pressure the transitions to the lamellar gel phase L_β are observed from 33 °C to 36 °C and from 40 °C to 43 °C in dispersions of DMPC/MA and DPPC/PA, respectively. When chain melting occurs, the inverted hexagonal phase is found to be the stable liquid-crystalline phase in DPPC/PA (1:2) dispersions, whereas in DMPC/MA (1:2) dispersions the Q^P_{II} phase is observed in coexistence with the H_{II} phase. In DMPC/MA (1:2) dispersions the lamellar L_α phase can be observed under non-equilibrium conditions after pressure jumps over the L_β to H_{II}/Q^P_{II} transition [49]. We investigated the pressure dependence of the lattice constant of the various phases in DMPC/MA and DPPC/PA (1:2) dispersions. Figure 10 shows the lattice constants of the L_β and H_{II} phase of DPPC/PA

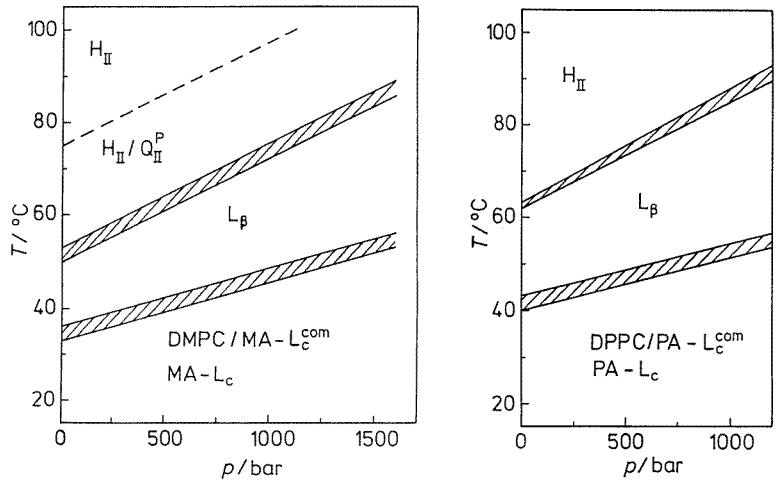

Figure 9. T,p phase diagrams of aqueous dispersions (a) of DMPC/MA (1:2) and (b) of DPPC/PA (1:2) in excess water.

(1:2) as a function of pressure for selected temperatures. The hexagonal lattice constant first increases with pressure (at a rate of about 5 Å kbar^{-1}) but then decreases drastically (8 Å) when the phase transition to the gel phase occurs. This unusual behaviour of the hexagonal lattice constant is assumed to be caused by the coexistence of the two phases. To address this problem, we determined the lattice constant of the hexagonal phase as a function of the molar ratio of the lecithin/fatty acid mixture. With increasing content of PA, $a(\mathrm{H}_{II})$ drastically decreases, e.g. from 59 Å at mole fraction $x_{PA} = 0.6$ to 50 Å at $x_{PA} = 0.8$ and $T = 75\,^{\circ}$C. Also results on other PC/FA systems show that the hexagonal lattice constant strongly depends on the lecithin/fatty acid ratio. It is thus possible to explain the observed behavior of $a(\mathrm{H}_{II})$ in the phase transition region with a variation of the lecithin/fatty acid ratio, which would be in accordance with the Gibbs phase rule. These data clearly show that, by changing lipid composition, curvature and thus fusogenicity of lipid membranes can easily be tuned. It is a generally observed phenomenon that when two amphiphiles of different character are present, it permits their relative concentrations to fluctuate, thus extending the polymorphism by the possibility of inhomogeneous interfacial curvatures.

2.2.1. Phase-separated lipid mixtures. There is considerable controversy regarding the lateral organization of lipid mixtures [61–65]. To understand the diverse effects of the presence of several components, studies of membranes composed of two components have been carried out. To address this problem, we used small-angle neutron scattering (SANS) experiments in combination with the H/D contrast variation technique [65]. We investigated mixtures where both components are saturated phospholipids of different acyl chain-length, such as DMPC(di-C_{14})/DSPC(di-C_{18}) dispersions. The range of momentum transfers $Q = (4\pi/\lambda)\sin\Theta$ (2Θ scattering angle, λ wavelength of radiation) covered by the neutron diffraction experiment was $4 \times 10^{-3} < Q$ (Å^{-1}) $< 1 \times 10^{-1}$. The scattering cross section density of the D_2O/H_2O solvent mixture was adjusted to that of an equimolar DMPC(d_{54})/DSPC mixture, assuming a homogeneous distribution of the two components. Under these so-called matching conditions, the scattering is determined by large-scale

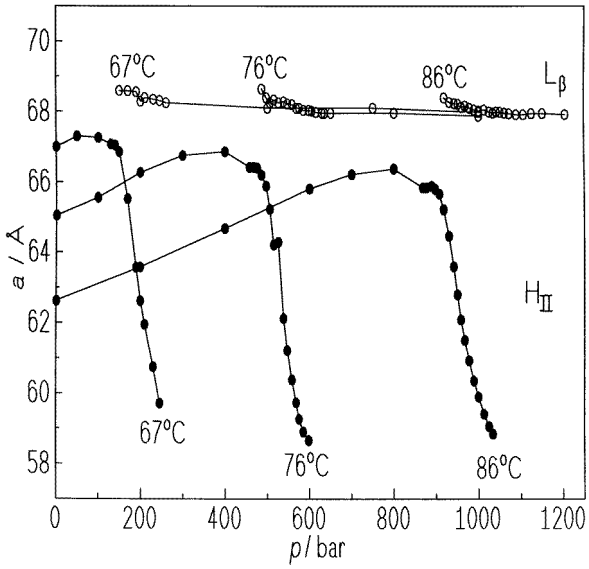

Figure 10. Pressure dependence of the lattice constants of the L_β and H_{II} phase of DPPC/PA (1:2 in 75 wt% H_2O) at 67 °C, 76 °C and 86 °C.

concentration fluctuations, only. The differential scattering cross-section of the sample can be written as

$$\frac{d\Sigma}{d\Omega} = n_p \Delta\rho^2 V_p^2 P(Q) S(Q) \tag{6}$$

where n_p denotes the number density of lipid molecules, V_p their volume, $\Delta\rho = \rho_p - \rho_s$ the contrast, i.e., the difference in mean scattering-length density of the particles (ρ_p) and the solvent (ρ_s) respectively. $P(Q) = \langle |F(Q)|^2 \rangle$ with the form factor $F(Q)$ of the particles, and $S(Q)$ is the structure factor describing the spatial distribution of the particles.

The temperature–pressure–concentration phase diagram of the DMPC/DSPC aqueous lipid dispersion has recently been determined by differential thermal (DTA) analysis [66]. The phase diagram of the mixture is depicted in figure 11. With increasing temperature, the gel, two-phase and fluid coexistence region of the mixture is shown. Deviations from ideal mixing behaviour of the two lipid components are considerable, as can already be inferred from the broad gel–fluid coexistence region. The system is close to a gel–gel immiscibility. The transition temperatures T_m of the pure lipid components at ambient pressure are 55 °C for DSPC-h_{88} and 24 °C for DMPC-h_{72}, respectively. Deuteration lowers the phase-transition temperature of DMPC-d_{54} by about 4 °C and thus shifts the solidus line of the two-phase region of the mixture to slightly lower temperatures. With increasing pressure, the two-phase coexistence region is shifted towards higher temperatures, and the shape of the phase diagram is essentially unaltered. A shift of about 22 °C $kbar^{-1}$ is observed, similar to the slope $(dT/dp)_{coex}$ of the coexistence line of the gel to fluid transition of the saturated phospholipid components. Only within the two-phase region does significant small-angle scattering occur (figure 12), and the $\ln(d\Sigma/d\Omega)$–$\ln(Q)$ plots give a straight line over the whole Q-range covered. Such a power-law scattering is indicative of a fractal-like behaviour of the sample. For fractal objects in three dimensions that are self-similar over a range of length scales, the structure factor reduces to $S(Q) \propto Q^{-D_m}$ when $\zeta^1 < Q < d^{-1}$ [67]. D_m is the fractal dimension of the object (mass fractal) which relates the size r of the object to its

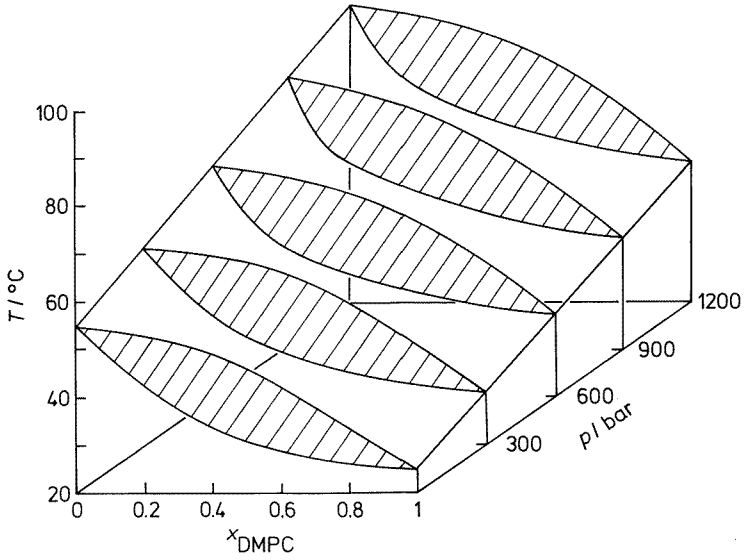

Figure 11. T,x phase diagram of the binary lipid mixture DMPC/DSPC 1:1 (mol:mol) in excess water as a function of pressure.

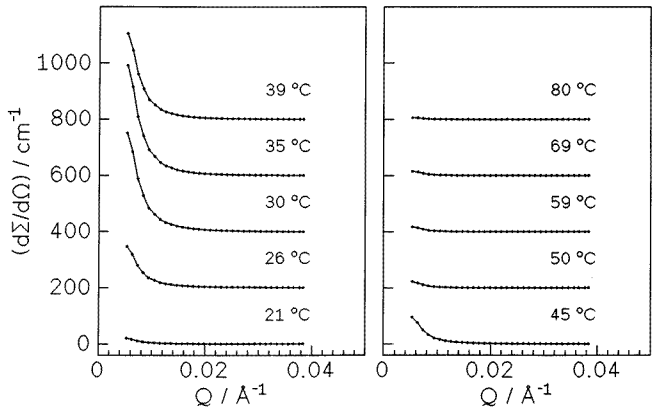

Figure 12. SANS curves of a contrast matched DMPC(d_{54})/DPPC 1:1 (mol:mol) dispersion at selected temperatures ($p = 1$ bar).

total mass ($m \propto r^{D_m}$, $0 < D_m < 3$), ζ is the cut-off distance of the fractal object and d is the characteristic size of the individual scatterers. For scattering from three-dimensional objects with fractal surface (surface fractals), having the property that the surface area varies as a non-integer power of length, the power law exponent is $-(6 - D_s)$, where D_s is the fractal dimension of the surface ($2 \leqslant D_s < 3$). $D_s = 2$ represents a smooth surface. From the log–log plot of the data in figure 12 a slope of -3.3 ± 0.1 is obtained, which yields a surface fractal dimension of $D_s = 2.7 \pm 0.1$. For the two-phase coexistence region at 1000 bar, a similar slope of about -2.8 ± 0.2 has been observed in the $\ln(\mathrm{d}\Sigma/\mathrm{d}\Omega)$–$\ln(Q)$ plot. Thus, in the two-phase region, large-scale fluctuations abound, which can be characterized as a nonuniform system of coexisting clusters exhibiting fractal-like behaviour. The fluctuations

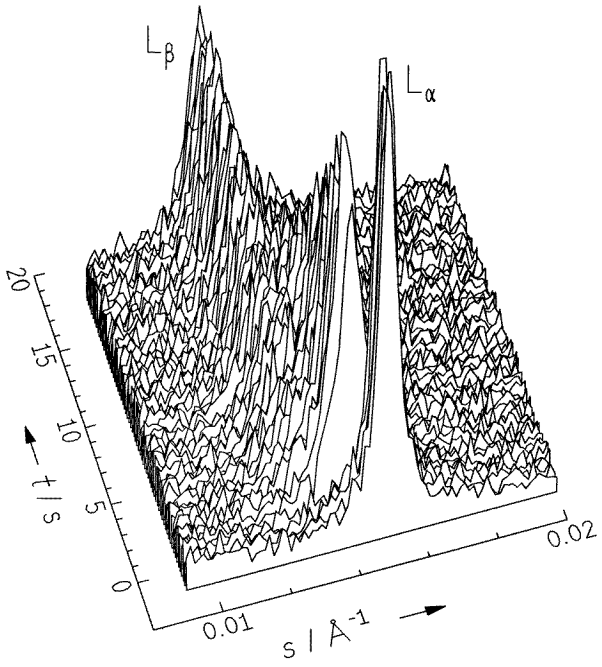

Figure 13. Selected diffraction patterns of DEPC in excess water after a pressure jump from 200 to 370 bar at 18 °C.

seen lie in the range 200–1500 Å. For these mixtures we conclude that the phase-separated domains constitute three-dimensional domains with fractal surface, $D_s = 2.7$. The fluid and gel islands in neighbouring bilayers seem to be strongly correlated. The phase-separated regions in an individual bilayer are two-dimensional islands with $(D_s - 1)$-dimensional fractal boundary. The high dimension of this boundary, 1.7, implies a low line tension between the fluid and gel phase. Finally, we note that the interpretation of the phase-separated domains as surface fractals is equivalent to a power-law distribution of droplets of one phase in the other.

These results imply that the membrane structure in the gel–fluid coexistence region departs strongly from what is expected from the equilibrium phase diagram and which is generally observed for macroscopically large systems (large gel and fluid domains separated by smooth boundaries). The heterogeneous membrane structure observed in the two-phase coexistence region might be due to interfacial wetting effects such as those suggested recently from computer simulations [68, 69]. In these calculations, the interface between coexisting gel and fluid phases domains is found to be enriched by one of the lipid species, leading to a decrease of the interfacial tension and hence to a stabilization of non-equilibrium lipid domains. These and further results on similar binary lipid systems suggest that such heterogeneous and fractal-like domain morphologies might be a common phenomenon. Depending on the acyl-chain mismatch of the lipid components, the clusters scatter like surface or mass fractals, implying that gel and fluid domains are correlated across many bilayers, and that segregation into a minority and majority phase occurs, respectively [70]. These results will certainly have also drastic consequences for the interpretation of dynamic properties of membrane components.

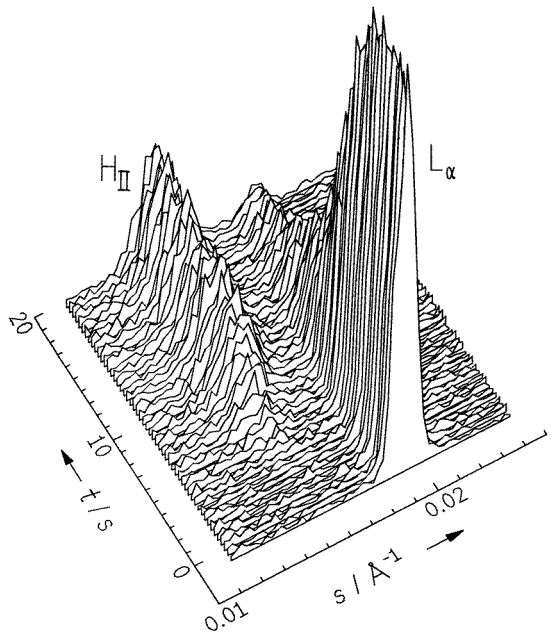

Figure 14. Selected diffraction patterns of DOPE in excess water after a pressure jump from 300 to 110 bar at 20 °C.

2.3. Kinetics of lipid phase transformations

Although the static structure and phase behaviour of many lipid systems is rather well established, considerable lack of knowledge exists regarding the understanding of the kinetics and mechanisms of lipid phase transformations. We used the synchrotron x-ray diffraction technique to record the temporal evolution of the structural changes after induction of the phase transition by a pressure-jump across the phase boundary [49]. In the following we will discuss two representative examples. First we present pressure-jump experiments carried out in DEPC/water dispersions to study the L_β/L_α transition. Selected SAXS diffraction patterns at 18 °C after a pressure-jump from 200 to 370 bar are depicted in figure 13. An intermediate structure is clearly observable. The first-order Bragg reflection of the initial L_α ($a = 66$ Å) phase vanishes in the course of the pressure-jump (5 ms). The first diffraction pattern collected after the pressure-jump exhibits a Bragg reflection of a new lamellar phase L_x with a larger a-value, which increases with time. The lattice constant of the L_β phase formed is 78 Å. The transition is complete after about 15 s. In equilibrium measurements, no such intermediate lamellar structure is detectable (see figure 2). Interestingly, the pressure-jump amplitude has a significant influence on the lifetime and a-value of the intermediate structure. It decreases with the distance from the phase transition line. In the depressurization ($L_\beta \rightarrow L_\alpha$) direction, the lifetime of the intermediate L_x phase is found to be significantly shorter.

Experiments for investigating the lamellar/H_{II} transition kinetics have been performed on DOPE dispersions. Figure 14 shows the diffraction pattern at 20 °C after a pressure-jump from 300 to 110 bar. In this case, a two-step mechanism is observed. Interestingly, it has been found that successive temperature-jumps lead to an acceleration of the phase transition kinetics. The half transition time decays from 8.5 s for the first pressure jump to 5.3 s after

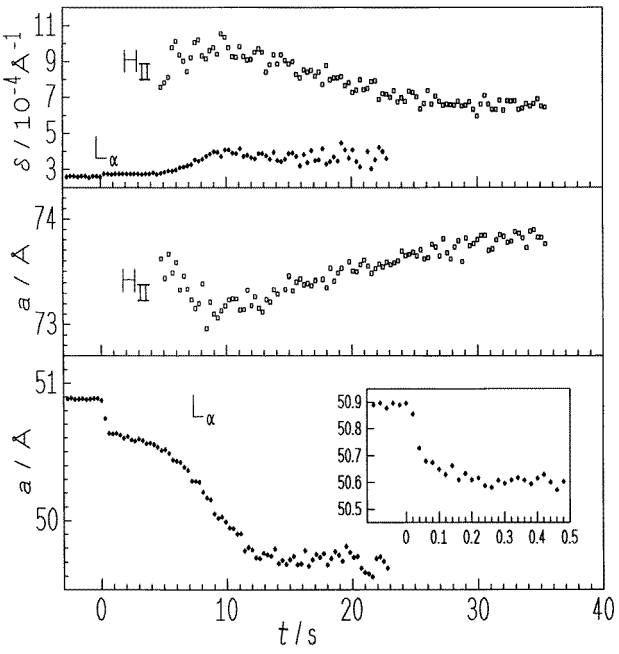

Figure 15. Lattice constants a and half-widths δ of the first-order Bragg reflections of the L_α phase and the H_{II} phase of DOPE in excess water after a pressure-jump from 300 to 110 bar at 20 °C.

the fourth jump. An induction period of several s is observed after the pressure jump before the first Bragg reflections of the newly formed H_{II} phase appears. Upon successive pressure cycles, this induction period decreases, whereas the rate of phase transformation as obtained from the intensity curves stays essentially constant. An explanation for this phenomenon might be the formation of defect structures which are formed during the pressure cycles and which have not healed out between successive pressure cycles. This observation also shows that the history of sample preparation plays an essential role in these kinds of study. With increasing pressure-jump amplitude, the induction period decreases and the rate of phase transfomation increases (e.g., 10%/0.6 s phase change for a 300 → 110 bar jump (induction period 5 s) and 10%/0.15 s phase change for a 300 → 1 bar pressure-jump (induction period 0.5 s)). Figure 15 shows the lattice constants and half-widths of the Bragg reflections of the L_α and H_{II} phase at 20 °C after a pressure-jump from 300 → 110 bar. After 20 ms the lattice constant of the L_α phase has decreased by 0.2 Å, probably due to fast conformational changes (probably on the ns time scale) of the lipid acyl chains. After that fast process $a(L_\alpha)$ decreases slowly to 50.6 Å after 250 ms. After the induction period the Bragg reflection of the H_{II} phase appears. $a(H_{II})$ first decreases slightly, and then increases again due to water uptake by 0.5 Å up to 73.9 Å after about 25 s. At the same time as the H_{II} phase is formed, $a(L_\alpha)$ decreases correspondingly. The decrease in half-width of the (10) reflection of the H_{II} phase with time might be due to the formation of an elongation and a denser packing of the micellar tubes forming the hexagonal structure. As the fully hydrated H_{II} phase needs much more water than the lamellar phase, and the lattice constant $a(H_{II})$ does not change significantly with time, one might assume that the necessary water uptake occurs within the defect structures being formed during the induction period. These structures do not lead to coherent scattering patterns, however.

Generally, as has also been found in studies of pressure- and temperature-jump induced phase transitions of other systems [49, 71, 72], the results show that the relaxation behaviour and the kinetics of lipid phase transformations drastically depend on the topology and symmetry of the lipid phases, as well as on the applied jump amplitude Δp. In most cases the rate of the transition is probably limited by the transport and redistribution of water into and in the new phase, rather than being controlled by the required time for a rearrangement of the lipid molecules. This can be inferred from lattice relaxation experiments in the lipid one-phase regions. For example, in the H_{II} phase of DOPE, lattice relaxation times are on the time scale 10–20 s, depending on Δp and T, which are about an order of magnitude slower than those in lamellar phases. The turtuosity factor of the different structures, especially in cases where non-lamellar (hexagonal and cubic [49]) phases are involved, is likely to control the different kinetic components. In addition, nucleation phenomena and domain size growth of the structures evolving might also play a significant role.

We conclude that pressure work on model membrane and lipid systems can yield a wealth of enlightening new information on the structure, energetics and phase behaviour of these systems, and on the transition kinetics between lipid mesophases. In addition, these results are of biological and biotechnological relevance.

Acknowledgments

Financial support from the Deutsche Forschungsgemeinschaft (DFG), the Fonds der Chemischen Industrie and the DAAD (ARC) is gratefully acknowledged. We thank Drs J Seddon and R Templer for many valuable discussions.

References

[1] Seddon J M 1990 *Biochim. Biophys. Acta* **1031** 1
[2] Seddon J M and Templer R H 1993 *Phil. Trans. R. Soc.* A **344** 377
[3] Cevc G and Marsh D 1987 *Phospholipid Bilayers* (New York: Wiley)
[4] Cevc G (ed) 1993 *Phospholipids Handbook* (New York: Dekker)
[5] Lipowski R and Sackmann E (eds) 1995 *Structure and Dynamics of Membranes* vols 1A, 1B (Amsterdam: Elsevier)
[6] Winter R, Landwehr A, Brauns Th, Erbes J, Czeslik C and Reis O 1996 *High Pressure Effects in Molecular Biophysics and Enzymology* ed J L Markley, D B Northrop and C A Royer (Oxford: Oxford University Press) p 274
[7] Winter R and Pilgrim W C 1989 *Ber. Bunsenges. Phys. Chem.* **93** 708
[8] Braganza L F and Worcester D L 1986 *Biochemistry* **25** 2591
[9] Böttner M, Ceh D, Jacobs U and Winter R 1994 *Z. Phys. Chem.* **184** 205
[10] Chong P-L G and Weber G 1983 *Biochemistry* **22** 5544
[11] Wong P T T, Siminovitch D J and Mantsch H H 1988 *Biochim. Biophys. Acta* **947** 139
[12] Driscoll D A, Jonas J and Jonas A 1991 *Chem. Phys. Lipids* **58** 97
[13] Landwehr A and Winter R 1994 *Ber. Bunsenges. Phys. Chem.* **98** 214
[14] So P T C, Gruner S M and Shyamsunder E S 1993 *Phys. Rev. Lett.* **70** 3455
[15] Reis O, Winter R and Zerda T W 1996 *Biochim. Biophys. Acta* **1279** 5
[16] Czeslik C, Winter R, Rapp G and Bartels K 1995 *Biophys. J.* **68** 1423
[17] Cheng A, Mencke A and Caffrey M 1996 *J. Phys. Chem.* **100** 299
[18] Duesing P M, Seddon J M, Templer R H and Mannok D A 1997 *Langmuir* **13** 655
[19] Bonev B B and Morrow M R 1995 *Biophys. J.* **69** 518
[20] Czeslik C, Reis O, Winter R and Rapp G 1998 *Chem. Phys. Lipids.* **91** 135
[21] Lindblom G and Rilfors L 1989 *Biochim. Biophys. Acta* **988** 221
[22] Tate M W, Eikenberry E F, Turner D C, Shyamsunder E and Gruner S M 1991 *Chem. Phys. Lipids* **57** 147
[23] Erbes J, Czeslik C, Hahn W, Rappolt M, Rapp G and Winter R 1994 *Ber. Bunsenges. Phys. Chem.* **98** 1287
[24] Luzzati V, Vargas R, Mariani P, Gulik A and Delacroix H 1988 *J. Mol. Biol.* **229** 540

[25] Luzzati V 1995 *J. Physique* II **5** 1649
[26] Gruner S M 1987 *Liposomes, from Biophysics to Therapeutics* ed M J Ostro (New York: Dekker) p 1
[27] Chernomordik L, Kozlov M M and Zimmerberg J 1995 *J. Membrane Biol.* **146** 1
[28] Bouligand Y 1990 *Coll. Phys.* C **7** 35
[29] Mariani P, Luzzati V and Delacroix H 1988 *J. Mol. Biol.* **204** 165
[30] Luzzati V 1997 *Curr. Opin. Struct. Biol.* **7** 661
[31] Landh T 1995 *FEBS Lett.* **369** 13
[32] Charvolin J and Sadoc J-F 1996 *Phil. Trans. R. Soc.* A **354** 2173
[33] Hyde S T 1989 *J. Phys. Chem.* **93** 1458
[34] Templer R H, Seddon J M and Warrender N A 1994 *Biophys. Chem.* **49** 1
[35] Templer R H, Turner D C, Harper P and Seddon J M 1995 *J. Physique* II **5** 1053
[36] Templer R H 1995 *Langmuir* **11** 334
[37] Templer R H, Seddon J M, Duesing P M, Winter R and Erbes J 1998 *J. Phys. Chem.* at press
[38] Chung H and Caffrey M 1994 *Biophys. J.* **66** 377
[39] Chung H and Caffrey M 1994 *Nature* **368** 224
[40] Mariani P, Paci B, Bösecke P, Ferrero C, Lorenzen M and Caciuffo R 1996 *Phys. Rev.* E **54** 5840
[41] Helfrich W 1990 *Liquids at Interfaces (Les Houches Summer School Session XLVIII)* ed J Charvolin, J-F Joanny and J Zinn-Justin (Amsterdam: North-Holland)
[42] Rostain J C, Martinez E and Lemaire C (eds) 1989 *High Pressure Nervous Syndrome—20 Years Later* (Marseille: ARAS-SNHP)
[43] Balny C, Hayashi R, Heremans K and Masson P (eds) 1992 *High Pressure and Biotechnology (Colloque Inseram, 224)* (Montrouge: Libbey Eurotext)
[44] Winter R and Jonas J (eds) 1993 *High Pressure Chemistry, Biochemistry and Materials Science (NATO ASI C 401)* (Dordrecht: Kluwer)
[45] Macdonald A G 1986 *Topic in Lipid Research* ed R Klein and B Schmitz (London: Royal Society of Chemistry) p 319
[46] Macdonald A G 1984 *Phil. Trans. R. Soc.* B **304** 47
[47] Behan M K, Macdonald A G, Jones G R and Cossins A R 1992 *Biochim. Biophys. Acta* **1103** 317
[48] Czeslik C, Malessa R, Winter R and Rapp G 1996 *Nucl. Instrum. Methods* A **368** 647
[49] Erbes J, Winter R and Rapp G 1996 *Ber. Bunsenges. Phys. Chem.* **100** 1713
[50] Reis O and Winter R 1998 *Langmuir* **14** 2903
[51] Bernsdorff S, Wolf A, Winter R and Gratton E 1997 *Biophys. J.* **72** 1264
[52] Czeslik C 1997 *PhD Thesis* University of Dortmund
[53] Chang E L and Yager P 1983 *Mol. Cryst. Liq. Cryst.* **98** 125
[54] Shyamsunder E, Gruner S M, Tate M W, Turner D C, So P T C and Tilcock C P S 1988 *Biochemistry* **27** 2332
[55] Siegel D P 1993 *Biophys. J.* **65** 2124
[56] Turner D C, Wang Z-G, Gruner S M, Mannock D A and McElhaney R N 1992 *J. Physique* II **2** 2039
[57] Anderson D M, Gruner S M and Leibler S 1988 *Proc. Natl Acad. Sci. USA* **85** 5364
[58] Koynova R D, Tenchov B G, Quinn P J and Laggner P 1988 *Chem. Phys. Lipids* **48** 205
[59] Koynova R D, Boyanov A I and Tenchov B G 1987 *Biochim. Biophys. Acta* **903** 186
[60] Koynova R D, Tenchov B G and Rapp G 1997 *Chem. Phys. Lipids* **88** 45
[61] Almeida P F F, Vaz W L C and Thompson T E 1992 *Biochemistry* **31** 7198
[62] Morrow M R, Srinivasan R and Grandal N 1991 *Chem. Phys. Lipids* **58** 63
[63] Schmidt G and Knoll W 1985 *Ber. Bunsenges. Phys. Chem.* **89** 36
[64] Sankaram M B and Thompson T E 1992 *Biochemistry* **31** 8258
[65] Czeslik C, Erbes J and Winter R 1997 *Europhys. Lett.* **37** 577
[66] Landwehr A and Winter R 1994 *Ber. Bunsenges. Phys. Chem.* **98** 1585
[67] Pfeifer P and Obert M 1989 *The Fractal Approach to Heterogeneous Chemistry—Surface, Colloids, Polymers* ed D Avnir (Chichester: Wiley) p 11
[68] Jørgensen K, Sperotto M M, Mouritsen O G, Ipsen J H and Zuckermann M J 1993 *Biochim. Biophys. Acta* **1152** 135
[69] Jørgensen K and Mouritsen O G 1995 *Biophys. J.* **95** 942
[70] Winter R, Gabke A, Czeslik C and Pfeifer P submitted
[71] Laggner P, Kriechbaum M and Rapp G 1991 *J. Appl. Cryst.* **24** 836
[72] Caffrey M 1987 *Biochemistry* **26** 6349